

Journal of Materials Chemistry C

Accepted Manuscript



This is an *Accepted Manuscript*, which has been through the Royal Society of Chemistry peer review process and has been accepted for publication.

Accepted Manuscripts are published online shortly after acceptance, before technical editing, formatting and proof reading. Using this free service, authors can make their results available to the community, in citable form, before we publish the edited article. We will replace this *Accepted Manuscript* with the edited and formatted *Advance Article* as soon as it is available.

You can find more information about *Accepted Manuscripts* in the [Information for Authors](#).

Please note that technical editing may introduce minor changes to the text and/or graphics, which may alter content. The journal's standard [Terms & Conditions](#) and the [Ethical guidelines](#) still apply. In no event shall the Royal Society of Chemistry be held responsible for any errors or omissions in this *Accepted Manuscript* or any consequences arising from the use of any information it contains.



Nanoporous Gyroid Metal Oxides with Controlled Thickness and Composition by Atomic Layer Deposition from Block Copolymer Templates

Received 00th January 20xx,
Accepted 00th January 20xx

DOI: 10.1039/x0xx00000x

www.rsc.org/MaterialC

Wei-Chun Ma^a, Wei-Shiang Huang^a, Ching-Shun Ku^{*b} and Rong-Ming Ho^{*a}

Herein, we aim to suggest an approach for the fabrication of nanoporous gyroid metal oxides with well-controlled tubular thickness and composition as well as film thickness by templated atomic layer deposition (ALD). Dip-coating method is used to prepare gyroid polystyrene-*block*-poly(L-lactide) (PS-PLLA) thin films with uniform film-thickness at micrometer scale. Polymer with gyroid nanochannels can be obtained by hydrolysis of PLLA blocks in the PS-PLLA film, which served as a template for ALD. Templated ALD is carried out to fabricate PS/ZnO gyroid nanohybrids. After removal of the PS matrix, nanoporous gyroid ZnO can be obtained. Controlled diffusion length (i.e., film thickness) for the growth of the nanoporous ZnO can be attained by tuning the exposure time of precursor gas whereas controlled tubular thickness can be achieved through the control of ALD cycles. Moreover, alternating reaction processes to introduce various precursor gases for templated ALD were carried out for the formation of core-shell metal oxide alloys, e.g. Al₂O₃@ZnO, demonstrating the feasibility to create nanoporous gyroid networks with controlled composition. As a result, micrometer-thick nanoporous gyroid alloys with large specific surface area and high porosity as well as superior mechanical properties can be successfully fabricated.

Introduction

Nanoporous metal oxides, in particular with network textures, have a wide variety of desiring and useful characteristics. Usually, nanoporous metal oxides can be prepared by sintering of packed nanoparticles at which between inter-particle gaps identify the pore structure that resulting in a wide pore size distribution and ill-defined pore morphology. To achieve well-defined pore texture, nanoporous metal oxides can be fabricated by a surfactant-aided sol-gel process (a soft-template approach), followed by removal of the surfactant (i.e., the template materials); however, it is often difficult to fabricate large-scale ordered structures, in particular in the thin-film state, since the removal of the surfactant may result in the imperfection of templated texture.¹ By contrast, a hard-template approach is exploited by using a pre-made templates for the syntheses of well-ordered nanoporous materials with extended lateral ordering even after removal of the templates.²⁻⁵ For the use of polymer templates, it is definitely advantageous to give well-defined texture, particularly in the thin-film state, resulting from

the simple processing of polymeric materials.⁶

In recent decades, self-assembly of block copolymers (BCPs) has been broadly examined as a consequence of their capability to self-assemble into a selection of ordered nanostructures through microphase separation.⁷⁻¹⁰ By taking advantage of the molecular engineering of synthetic BCPs, the self-assembled materials provide promising characteristics for applications in nanomaterials. One eminent approach is the fabrication of nanoporous templates using the self-assembled block copolymers through removal of constituted components in BCPs. With the degradable character of BCPs, well-ordered nanoporous polymers can be prepared through ozonolysis,^{11,12} UV degradation,¹³ or reactive ion etch.¹⁴ Polylactide-containing BCPs (such as polystyrene-*b*-poly(D,L-lactide) (PS-PLA)¹⁵ and polystyrene-*b*-poly(L-lactide) (PS-PLLA)¹⁶) are also highly suited to serve the purpose through the simple hydrolytic treatment. Around all of the nanostructures due to the BCP self-assembly, one of the most attractive morphologies is double gyroid because of its unique geometry with well-ordered network texture which can be exploited for practical applications. The basic shape of the gyroid is a three-fold junction of three arms, in which each arm is connected to another set of three arms that are each themselves rotated to form a 3D network.^{17,18} For a double gyroid phase, it is composed of a bicontinuous but independent, interpenetrating triply networks in a three-dimensional space.¹⁹⁻²¹ For a degradable block copolymers with gyroid nanostructure, it is a perfect candidate to serve as a template after the selective degeneration of minor phase to create fully interconnected nanochannels for templated reactions, such as sol-gel reaction,²²⁻²⁴ electrochemical deposition,²⁵⁻³⁰ electroless plating,³¹⁻³⁵ and atomic layer deposition (ALD),^{36,37} giving well-

^a Department of Chemical Engineering, National Tsing Hua University, Hsinchu 30013, Taiwan, R.O.C.

^b National Synchrotron Radiation Research Center, 101 Hsin-Ann Road, Hsinchu Science Park, Hsinchu 30076, R.O.C.

† Electronic Supplementary Information (ESI) available: [details of any supplementary information available should be included here]. See DOI: 10.1039/x0xx00000x

* To whom correspondence should be addressed: rmho@mx.nthu.edu.tw and csku@nsrrc.org.tw

defined nanohybrids with accurately controlled structure. After removal of the template, well-ordered nanoporous materials with

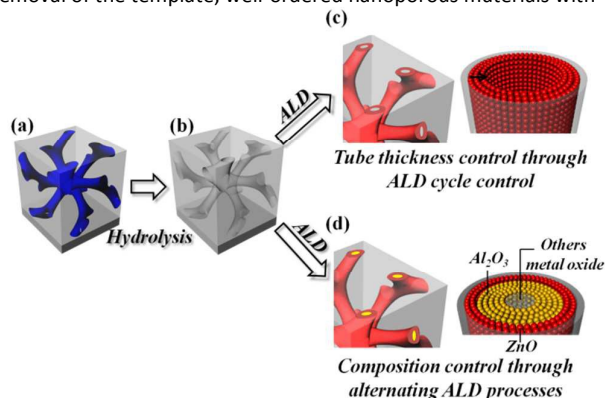


Fig. 1 Schematic illustration for the fabrication of nanoporous gyroid metal oxides and alloys from BCP template: (a) gyroid-forming PS-PLLA film from dip coating; (b) nanoporous PS with gyroid nanochannels; (c) tube thickness control through ALD cycle control; (d) composition control through alternative ALD processes.

network textures can be fabricated,⁵ giving a broad variety of applications such as photonic crystals,^{38,39} catalysts,²⁴ ceramic membranes,²⁵ and hybrid solar cells.²⁶

Note that templated electroless plating is practicable to fabricate metal-based nanomaterials without applying the electric field on reducing metal ions for electrochemical deposition. The templated sol-gel reaction is a simple process to produce a variety of ceramic nanomaterials because of the sophisticated development in sol-gel sciences. However, it is challenging to fabricate tubular and core-shell structures through templated syntheses, in particular with controlled nanoscale dimension. In this study, we aim to use hard templates derived from hydrolyzed polylactide-containing BCPs with double gyroid texture to demonstrate the feasibility in the fabrication of tubular and core-shell structures through the control of ALD cycles and alternating ALD processes, respectively. Consequently, nanoporous tubular ZnO and core-shell metal oxide alloys, e.g. Al₂O₃@ZnO, are fabricated, giving free-standing, nanoporous gyroid metal oxides with specific functions for a broad range of appealing applications. Accordingly, with the easy formation of polymer thin film, micrometer-thick nanoporous gyroid alloys with high porosity and large specific surface area as well as superior mechanical properties can be successfully fabricated using self-assembled BCP as a template for ALD reaction. Tubular hollow structures have a wide variety of attractive and useful characteristics, in particular having a great advantage of providing the high transparent property in the photonic applications, and to enhance the air-material interfacial area for providing the superior electrochemical performances as electrode materials.^{40,41} The core-shell nanostructure have received increasing attention because of their tunable physical and chemical properties through controlling composition and relative sizes of core and shell, giving promising applications in many research areas.⁴²

Fig. 1 illustrates the processes for the fabrication of well-ordered nanoporous gyroid metal oxides from BCP templates. A double gyroid structure, consisting of PLLA networks in a PS matrix, can be formed after solvent-annealing thin film from dip coating process (Fig. 1a). Subsequently, nanoporous gyroid thin films with micrometer thickness can be obtained from the self-assembly of PS-PLLA followed by the hydrolysis of PLLA blocks (Fig. 1b). The nanoporous gyroid PS is used as a template for ALD to fabricate gyroid nanohybrids with well-defined PS/ZnO nanotubes and PS/Al₂O₃@ZnO (i.e., core-shell metal oxide alloys in PS matrix). Controlled diffusion length (i.e., film thickness) for the growth of the nanoporous ZnO can be obtained by tuning the exposure time to precursor gas whereas tube thickness control can be achieved through the control of ALD cycle (Fig. 1c). Moreover, alternating reaction processes to introduce various precursor gases for templated ALD can be carried out for the formation of core-shell metal oxide alloys, e.g. Al₂O₃@ZnO, demonstrating the feasibility to fabricate nanoporous gyroid alloys with controlled composition (Fig. 1d). After calcination to remove the PS template, nanoporous gyroid metal oxide nanotubes and core-shell metal oxide alloys with high porosity and large specific surface area can be successfully fabricated. Because of the intrinsic texture of gyroid with free-standing and self-supporting characters, ZnO nanotubes with 3D network texture, and the new-type structures with Al₂O₃@ZnO core-shell metal oxide alloys are fabricated. The Al₂O₃@ZnO core-shell metal oxide alloys are particularly interesting in the designs of optical devices with high mechanical properties.

Experimental methods

Synthesis of PS-PLLA BCPs.

The PS-PLLA BCPs were prepared by sequential living polymerization method using a double-headed initiator. Detailed synthetic routes of the PS-PLLA preparation were described in our previous reports.⁴³ The number-average molecular weight and the molecular weight distribution of the samples were determined by GPC. The polydispersity index (\bar{M}_w) of PS-PLLA was determined by GPC and the numbers of L-LA repeating units vs. styrene repeating units were determined by ¹H NMR analysis. The number-average molecular weights of the PS, the PLLA, and the \bar{M}_n of the PS-PLLA are 32000 g mol⁻¹, 22000 g mol⁻¹, and 1.21, respectively. The volume fraction of PLLA, f_{PLLA}^v , is thus calculated as 0.36 by assuming that the densities of PS and PLLA are 1.02 and 1.248 g cm⁻³, respectively.

Preparation of Thin Film.

Thin-film samples of the PS-PLLA were prepared by dip coating from dichloromethane (CH₂Cl₂) at room temperature. PS-PLLA was first dissolved in CH₂Cl₂ at a concentration of 15 wt%. PS-PLLA thin film was fabricated by a dip coating technique onto Si wafer substrates. Thin film samples was then transferred in a vial (150 ml) which is encased the 20 ml dichloromethane and sealed well having punch holes for the evaporation of the solvent. In order to minimize the formation of the defects and grain boundaries, the slow

evaporation of the solvent was carried out. After two weeks for drying, the PS-PLLA thin films can be obtained. The samples were

further dried in vacuum oven for three days at 50 °C so as to

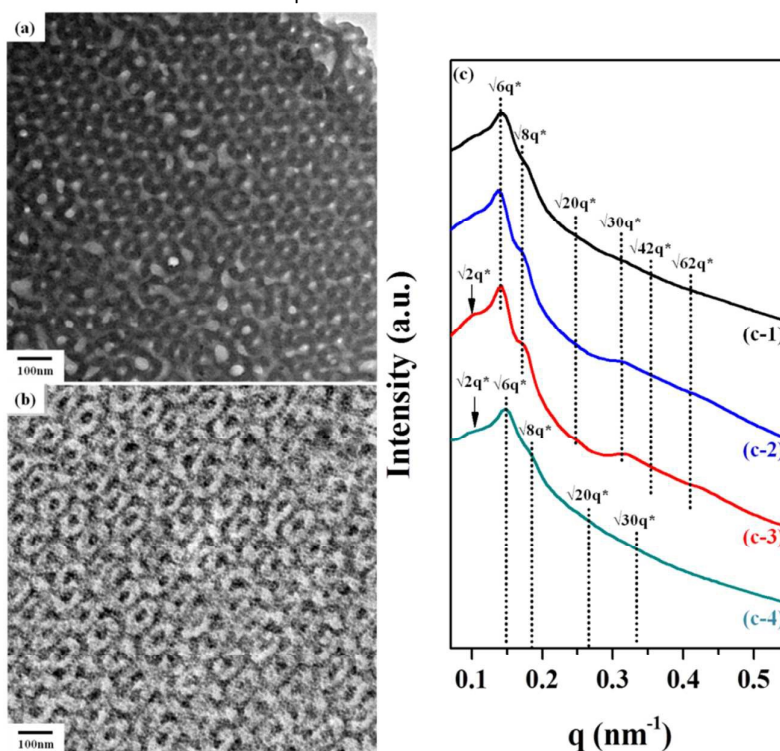


Fig. 2 (a) TEM micrograph of the gyroid-forming PS-PLLA thin film with RuO₄ staining along the [111] projection. (b) TEM micrograph of PS/ZnO gyroid nanohybrids fabricated by 100 ALD cycles. (c) One-dimensional SAXS profiles of (c-1) gyroid-forming PS-PLLA thin film; (c-2) nanoporous PS template after removal of minor PLLA blocks from the gyroid phase PS-PLLA; (c-3) PS/ZnO nanohybrids; (c-4) nanoporous gyroid ZnO.

remove the residual solvent. For thin film formation, the well-oriented microphase-separated nanostructures can be obtained. As a result, the well oriented BCP nanostructures were achieved. It is known that aliphatic polyesters can be hydrolytically degraded because of the unstable character of the ester group. PS-PLLA samples were placed in NaOH/MeOH solution for 5 days to degrade PLLA blocks. After complete degradation of the PLLA, nanoporous PS templates with gyroid-forming channels were rinsed by the mixture of distilled water and methanol. Subsequently, samples were dried under vacuum at room temperature for 24 h.

Fabrication Processes of Atomic Layer Deposition.

The ALD is a chemical vapor deposition (CVD) technique which relies on surface self-limiting and alternative, and irreversible gas phase to solid phase reaction of typically at least two compounds, which are repeated in a cyclic procedure. One conventional ALD cycle consists typically of four steps. The substrate usually contaminates with hydroxyls group on the surface which can react with the precursor. The first gas precursor inflows and reacts with substrate surface, i.e. chemisorption reaction, for first reactant (e.g. for ZnO compound usually is diethylzinc), followed by purge or evacuation to remove the unreacted precursor and by-products; second precursor is introduced into reactor and reacted with new

species, for second reactant (here is D. I. water), followed by purge or evacuation to remove the excess precursor and gases.

In this study, to improve the 3D padding ratio of Al₂O₃ and ZnO compounds into nanoporous gyroid, a novel ALD process (US patent 8105922B2) was used instead of conventional method as described as above. There is an additional process between each precursor pulse and purge to interrupt the pumping and to extend the immersion time of precursor. This immersion process, called "Stock" time, was achieved by a very fast actuator installed between pumping system and reaction chamber. This flow-rate interruption type ALD not only raises the filling ratio of complex 3D structure but also increases the crystallinity of compounds at very low reaction temperature, which is highly suitable for polymer templates.⁴⁴ The reaction temperature was kept at 50 °C and used the same temperature pure nitrogen gas (99.9999%) to purge the chamber between two-chemisorption reactions and to pump down the base pressure to 5×10⁻³ torr. The estimated growth rates from X-ray reflectivity for Al₂O₃ and ZnO layers are around 0.1 nm and 0.25 nm per ALD cycle, respectively.

Characterization.

Small-angle X-ray scattering (SAXS) experiments were conducted at the synchrotron X-ray beamline X27C at the National Synchrotron Radiation Research Center (NSRRC) in Hsinchu, Taiwan.

The wavelength of the X-ray beam was 0.155 nm. A MAR CCD X-ray detector (MAR USA) was used to collect the two-dimensional (2D) SAXS patterns. One-dimensional (1D) linear profile was obtained by

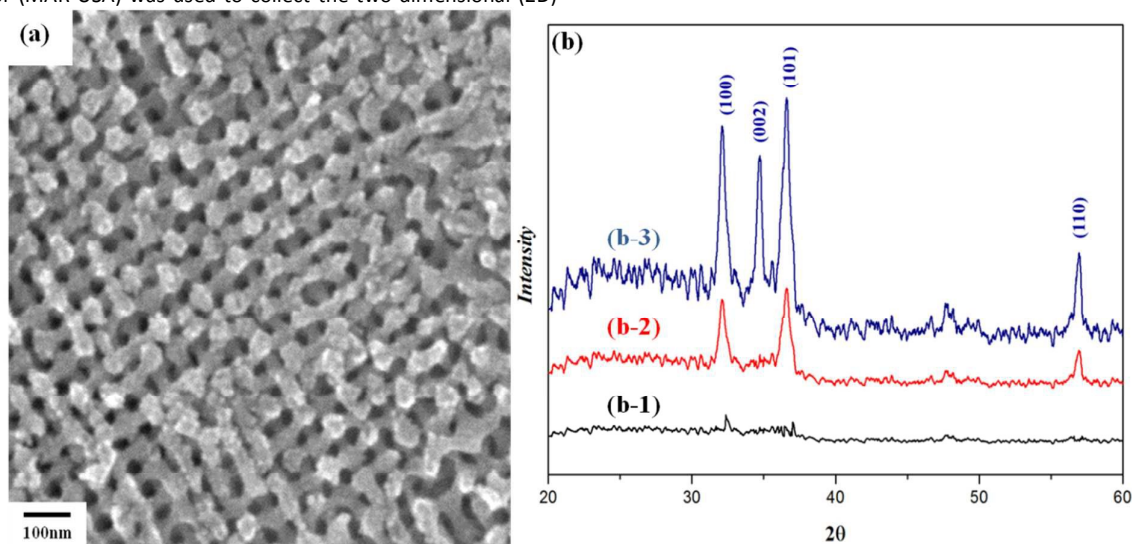


Fig. 3 (a) FESEM micrograph of gyroid ZnO fabricated through controlled calcination from the PS/ZnO gyroid nanohybrids. (b) 1D XRD profiles of the nanoporous ZnO with different conditions for thermal treatment: (b-1) without calcination (UV exposure); (b-2) ramped from 25 to 450 °C at 10 °C min⁻¹, held at 450 °C for 2 h, and then cooled from 450 to 25 °C at 10 °C min⁻¹; (b-3) ramped from 25 to 450 °C at 1 °C min⁻¹, held at 450 °C for 2 h, and then cooled from 450 to 25 °C at 1 °C min⁻¹.

integration of the 2D pattern. The scattering angle of the SAXS pattern was calibrated using silver behenate, with the first order scattering vector q^* ($q^* = 4\pi\lambda^{-1} \sin \theta$, where 2θ is the scattering angle) being 1.076 nm⁻¹. Bright-field transmission electron microscopy (TEM) images were obtained using the mass-thickness contrast with a JEOL JEM-2100 LaB₆ transmission electron microscope (at an accelerating voltage of 200 kV). Field-emission scanning electron microscopy (FESEM) observations were performed on a JEOL JSM-6700F using accelerating voltages of 1.5–3 keV. Before observations, the samples were sputter-coated with 2–3 nm of platinum to avoid the charge effect (the platinum coating thickness was estimated from a calculated deposition rate and experimental deposition time). To further confirm the structure of the ordered bicontinuous ZnO, we collected the powder of bicontinuous ZnO and performed a wide-angle X-ray diffraction (WAXD) experiment. The crystal structure of the as-prepared product was characterized by WAXD using a Rigaku Dmax 2200 X-ray diffractometer with Cu K α radiation ($\lambda = 0.1542$ nm). The scanning 2θ angle ranged between 20° and 60° with step scanning of 1° for 1 s.

Results and discussion, Experimental

Fabrication of gyroid nanohybrids and ordered nanoporous ZnO.

Fig. 2(a) shows the TEM micrograph of PS-PLLA thin film after solvent annealing at which the PS microdomain appears dark due to the staining of RuO₄ whereas the PLLA frameworks appear bright. The projection image suggests the formation results from a gyroid phase with the projection along the [111] direction. Fig. S1 shows the SEM image of the cross-section view of nanoporous PS template from Fig. 2(a) after hydrolysis, revealing the formation of

nanoporous 3 μ m thin film with well-ordered pore texture. The morphological results suggest that large-scale nanoporous polymeric thin film with uniform thickness can be successfully fabricated by dip-coating method followed by hydrolysis. The channels open from the surface of the film, and further extend through the entire film to the substrate (i.e., the through-pore texture) giving open-cell character for pore-filling process. The forming gyroid phase is further confirmed by one-dimensional SAXS results (Fig. 2(c-1)) at which the reflection peaks are found at the relative q values of $\sqrt{6}$: $\sqrt{8}$: $\sqrt{20}$: $\sqrt{30}$: $\sqrt{42}$: $\sqrt{62}$. From the primary reflection, the inter-domain spacing (211)_G (i.e., $d(211)_G$) was determined to be approximately 40.7 nm. According to the result (Fig. 2(c-2)), the reflections remain to suggest the retention of the gyroid texture after hydrolysis. The inter-domain spacing of the PS template was measured to be approximately 39.8 nm from the primary reflection, giving that the system takes a 2.6% shrinkage of its original size. Note that the discrepancy in the inter-domain spacing is attributed to the cavitation effect, resulting from a reduction in comparative dimension of the gyroid texture after hydrolysis.²⁴

It is noted that the selection of deposition temperature is critical for a successful templated ALD. For the deposition of ZnO, the temperature window is usually in the range of 80 to 150 °C to acquire the formation of crystalline ZnO with wurtzite structure but the PS template has a glass transition temperature of 90 °C. To avoid the template deformation problem due to high-temperature treatment, the deposition and reaction temperature was kept at 50 °C. A special thermal treatment was carried out by relatively slow cooling and heating in calcination processes to acquire the formation of wurtzite ZnO. Fig. 2(b) shows the TEM image of PS/ZnO gyroid nanohybrids from templated ALD reaction. The [111] projection image from TEM is an evidence for the formation of well-

defined PS/ZnO gyroid nanohybrids. The reversed mass-thickness contrast is attributed to the high atomic number of Zn that gives significant contrast from the PS template, resulting from the successful preservation of the gyroid texture after hydrolysis followed by templated ALD. Fig. 2(c-3) shows the scattering results from the nanohybrids at which the characteristic scattering profile for a gyroid structure at the relative q values of $\sqrt{2}:\sqrt{6}:\sqrt{8}:\sqrt{20}:\sqrt{30}:\sqrt{42}:\sqrt{62}$ can be found. Note that, in contrast to the small bump in the low q region in Fig. 2(c-2), a new peak attributed to $\sqrt{2}$ can be recognized. On the basis of our previous studies, it suggested that the network shifting due to the removal of the matrix, gives the reflections similar to a single gyroid phase with a space group of $I4_132$ to give the appearance of the $\sqrt{2}$ peak.⁴⁵ The interdomain spacing can be calculated from the two characteristic main peaks at a q value of $\sqrt{6}$ and $\sqrt{8}$, as constantly equivalent to the results from the PS template which was determined approximately 39.4 nm. Moreover, the different form factor and electron density contrast of the ZnO microdomain might result in the alteration in the q values. The texture information of the nanoporous gyroid ZnO can be further analyzed by SAXS (Fig. 2(c-4)); the scattering peaks occurs at the relative q values of $\sqrt{2}:\sqrt{6}:\sqrt{8}:\sqrt{20}:\sqrt{30}$. Although the deformation and collapse of the nanopores after calcination, resulting in the broadening of the characteristic reflections at high q range, the long range order of the ZnO metal oxide can be reasonably preserved as confirmed by the SAXS results. Accordingly, free-standing, nanoporous gyroid ZnO was successfully prepared, giving well-controlled ZnO with specific surface area and high porosity.

Fig. 3(a) shows the FESEM micrograph of nanoporous gyroid ZnO with well-defined, bi-continuous networks, reflecting the successful removal of the PS template. Also, no cracks can be observed, indicating that thermal expansion and cooling shrinking of materials on templated morphology can be successfully alleviated. As a result, free-standing, nanoporous gyroid-forming ZnO with precisely controlled texture was successfully fabricated. Fig. 3(b-1) shows the corresponding X-ray diffraction (XRD) pattern of the nanoporous gyroid ZnO, reflecting that the forming ZnO after the templated ALD followed by UV degeneration of PS is indeed in an amorphous state. As a result, the PS/ZnO gyroid nanohybrids were treated by calcined to degenerate the PS template and to crystallize the ZnO for better performance. Systematic examination of the crystallization behavior during calcination was conducted to realize the feature for increasing the densification and crystallinity.^{37,38} It is noted that crystallization of ZnO at high temperature (above 450 °C) will cause the deformation and pores collapse, especially in nanometer size. As a result, acquiring ZnO with wurtzite phase at high crystallinity without damaging the templated morphology requires dedicated calcination conditions, such as the control of chronological heating stages and rates as well as the corresponding calcination temperatures. To initiate the degeneration of the template and the crystallization of ZnO with wurtzite phase ZnO, it is necessary to treat the PS/ZnO nanohybrids at temperature over 400 °C. Accordingly, to acquire nanoporous gyroid ZnO with pure wurtzite phase, the PS/ZnO gyroid nanohybrids was calcinated at 450 °C in the air. To obtain the nanoporous gyroid ZnO with pure wurtzite phase in short time, the calcination condition go through the following protocol in the air

region: samples were fast heated from 25 to 450 °C at 10 °C min⁻¹; held at 450 °C for 2 h, and then fast cooled from 450 to 25 °C at 10 °C min⁻¹. Fig. 3(b-2) shows the corresponding 1D XRD pattern of prepared nanoporous ZnO, three diffraction peaks at $2\theta = 32.7^\circ$, 37.5° and 57.2° can be identified, indicating that the crystallinity is indeed enhanced by such a protocol for thermal treatment.⁴⁵ Yet, the fast heating and cooling will result in the distortion of the templated morphology due to fast thermal expansion and cooling shrinkage.⁴⁶ To alleviate the possible distortion of crystallized nanohybrids, the calcination was executed by comparatively slow cooling and heating. A improved calcination condition was thus suggested which was exposed in the air using the following protocol: samples were slowly heated from 25 to 450°C at 1°C min⁻¹; maintained at 450°C for 2h, and then slowly cooled from 450 to 25°C at 1°C min⁻¹. Fig. 3(b-3) shows the XRD profile of the nanoporous ZnO after the thermal treatment. All the diffractions peaks can be calculated on the basis of the lattice constants of a wurtzite phase at which $a = b = 3.2 \text{ \AA}$ and $c = 5.2 \text{ \AA}$, JCPDS card no. 36-1451, corresponding to the reflections of (100), (002), (101) and (110).

Templated ALD for thin films.

Unlike 1D structure, the 3D bi-continuous networks are much more complicate interconnected channels so that it requires longer exposure for the adsorption of precursors and longer purge time to remove the un-reactive precursors in order to achieve the deposition throughout the entire film thickness. For templated ALD reaction, the first step is to pore-fill the template with precursors. To examine the diffusion process for the pore-filling of precursor into the PS template before reaction, the precursor vapor was applied for different exposure times. While using relatively short exposure time (e.g. 1s), the film thickness of the PS/ZnO nanohybrids fabricated is too thin to satisfy the practical applications, indicating the diffusion length is too short to reach the entire sample thickness (Fig. S2). With further increasing the exposure time, the film thickness of the nanohybrids fabricated can be significantly enhanced. Eventually, the thickness will reach the maximum at 15 μm for 15s exposure time under the applied vapor pressure (Fig. 4(a)), suggesting that the diffusion length of the precursors can be increased by applied exposure time and then reach the maximum. These results indicate that the film thickness

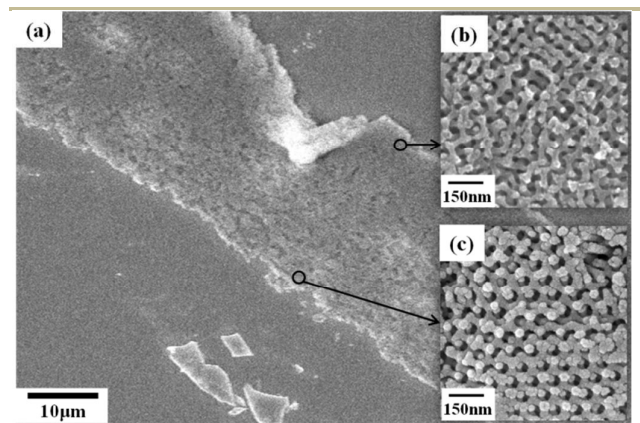


Fig. 4 FESEM micrographs of gyroid ZnO from deposition of ZnO by ALD into gyroid templates with exposure time at: (a) 15s. Well-ordered nanoporous gyroid ZnO after calcination can be found: (b) near the surface; (c) close to the bottom substrate.

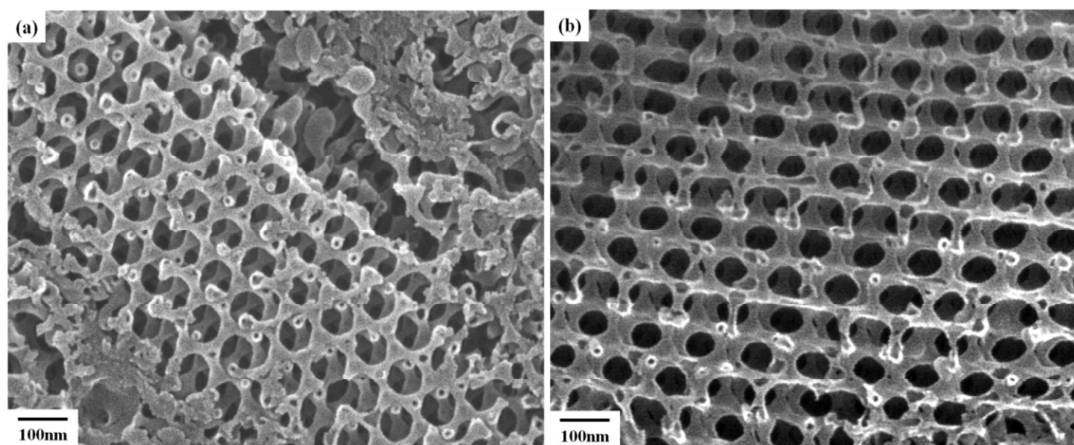


Fig. 5 FESEM micrographs of gyroid-forming ZnO nanotubes after removal of PS template by calcination after templated ALD with: (a) 40 ALD cycles; (b) 80 ALD cycles.

of the forming nanohybrids can be fine-tuned by the exposure time. Also, well-ordered nanoporous gyroid ZnO after calcination can be found in the whole sample thickness. As illustrated in Fig. 4(b) and 4(c), the gyroid texture can be clearly identified either near the surface or close to the bottom substrate, suggesting that the

templated synthesis is successful, and the forming gyroid is independent of the film thickness.

Tubular thickness control through ALD cycle control.

It is noted that the deposition rate of ZnO *via* ALD is approximately 2Å per cycle.^{47,48} As a result, it is legitimate to

suggest that the pore-wall thickness should be able to be adjusted by controlling the number of ALD cycle. The void channels diameter running through the gyroid-forming polymeric template is around 25 nm. As a result, after 80 cycles, the forming ZnO will be expected to give approximately 22 nm thickness on the inner wall of the template. Namely, it should be in a completely filled condition to form the preserved gyroid texture as evidenced in Fig. 3(a) at which a completed filled ZnO can be formed. With decreasing the cycle number of templated ALD, it is possible to bring the solid ZnO skeletons as ZnO tubes at which the tubular thickness can be controlled down to several nanometers. Fig. S3(a) displays the [110] projected TEM micrograph of the PS/ZnO gyroid nanohybrids after templated ALD with 40 ALD cycles without staining. In contrast to Fig. 2(b), a conformal thin layer of ZnO uniformly deposited on the inner walls of the PS template can be observed. After removal of PS templates by calcination, ZnO networks can be obtained (Fig. 5(a)). However, the acquired gyroid ZnO tube will experience collapse to give the resultant morphology as observed. We speculate that the thickness of the produced ZnO at 40 cycles is too thin to withstand the high temperature calcination, yielding a collapsed ZnO structure or porous defects. To avoid the calcination problem, the cycle number of the ALD increases to 80 cycles, Fig. S3(b) shows the projection TEM micrograph of the PS/ZnO DG nanohybrids fabricated by 80 ALD cycles. As shown, the interconnected network structure can be preserved and the pore size slightly decreases due to the increase of the ALD cycle number. After removal of PS template by calcination, the nanoporous gyroid ZnO tube networks with high surface area and porosity without defects can be obtained (Fig. 5(b)), suggesting that thicker tube wall gives the nanoporous gyroid ZnO tube with a stronger mechanical stability during calcination. Note that there is high possibility to cause the blocking of the nanopores due to the formation of ZnO from the surface of the thin film sample, and result in partial infiltration of

ZnO tube structure. To solve the problem, the ALD processes should be appropriately adjusted the precursor partial pressure, the exposure time, the template aspect ratio, and the surface chemistry composition of the template. Furthermore, adequate purge time for each half-cycle is crucial for the eradication of the undesired precursor and byproducts. The nanoporous gyroid networks have complicated morphologies of interconnected channels that gives extreme high specific surface area than conventional materials. Accordingly, to accomplish complete diffusion of the void channels in template and removal of the reaction products, the ALD process may need longer purge and pulse times. As a result, it is necessary to have a dedicated control of the reaction conditions for the templated ALD.

Characterization of tube thickness by reflectivity.

To quantitatively determine the growth thickness of the tubular ZnO from the control of ALD cycle, systematic examination of the forming ZnO from the templated ALD was carried out by using X-ray reflectometry (XRR). Fig. S4 shows the X-ray reflectivity data of the PS/ZnO gyroid nanohybrids in the film state on Si substrate from templated ALD with different cycles. On the basis of the recursive formalism of Parratt,⁴⁹ the physical parameters of the nanohybrids can be calculated from the fitting of the specular reflectivity at which the Mercury code was used to obtain the physical information of the nanohybrid thin film, including its thickness, roughness, and density.⁵⁰ Method of Analytic analysis tube thickness is based on the complex refractive index and critical angle (θ_c) given by

$$\tilde{n} = 1 - \delta + \beta i \quad (1)$$

where δ and β are corresponding to the dispersion and absorption. For frequencies large greater than the resonance frequencies of the atom, the δ can be given by the following expression

Table 1. Calculated results from the fitting of the X-ray reflectivity profile of the PS/ZnO gyroid nanohybrids.

	θ_c	ρ_e	ρ of film (g/cm^3)	ZnO filling ratio	Tube thickness (nm)
Flat ZnO	0.56	1.1×10^{24}	4.04		
30 cycles	0.35	4.5×10^{23}	1.61	0.23	6.0
60 cycles	0.45	7.3×10^{23}	2.60	0.48	8.6
90 cycles	0.55	1.1×10^{24}	3.82	0.78	11.1

$$\delta = \frac{e^2 \rho_e \lambda^2}{2 \epsilon_0 m (2\pi c)^2} = \frac{r_0 \lambda^2}{2\pi} \rho_e \quad (2)$$

where ρ_e is the electron density and r_0 is the Bohr atomic radius. By introducing small angle affinity and Snell's law, the critical angle (θ_c) can be represented as

$$1 - \delta = \cos \theta_c \approx 1 - \frac{\theta_c^2}{2} \quad (3)$$

$$\theta_c = \sqrt{2\delta} = \sqrt{\frac{r_0 \rho_e}{2\pi}} \lambda = 0.3 \times 10^{-14} \lambda \rho_e^{1/2} \quad (4)$$

the above function shows the relation between θ_c and ρ_e . It can be used to calculate the electron density and the film mass density

(ρ) through the θ_c . Subsequently, the ρ can be used to estimate the ZnO ratio because the ρ is contributed by density of ZnO (ρ_{ZnO}), PS templates (ρ_{PS}) and the air as shown below.

$$\rho = \rho_{\text{PS}} \times f_{\text{PS}} + \rho_{\text{ZnO}} \times f_{\text{ZnO}} + \rho_{\text{air}} \times f_{\text{air}} \quad (5)$$

$$f_{\text{ZnO}} + f_{\text{air}} = 0.36, f_{\text{PS}} = 0.64$$

f_{PS} is the volume fraction of PS, f_{ZnO} is the filling ratio of ZnO, and f_{air} is the volume fraction of air. ρ_{ZnO} is computed from the XRR profile of the flat ZnO deposited on Si wafer at 50°C (Fig. S4). The ZnO tube structure should completely occupy the hydrolyzed PLLA to give $f_{\text{ZnO}} + f_{\text{air}} = 0.36$. As a result, the tube thickness of the ZnO can be determined on the basis of the filling ratio of ZnO and the void channels diameter running through the PS template

(approximately 25 nm). The calculated physical parameters including the ZnO ratio, the packing ratio and the tube thickness are listed in Table 1. Consistent to the experimental results, the tube thickness from 30 cycle is 6.0 nm and the filling ratio is less than 0.3 that may result in the weak mechanical property as found. With the increase of the cycle number to 60, the filling ratio can be over 0.45 that provides better mechanical properties as expected (see below for details). The estimated results are almost consistent with the calculation on the basis of the growth rate of ZnO deposition *via* ALD with approximately 2 Å per cycle. Most interestingly, it is not a linear growth as expected at which the increasing rate of tube thickness is reduced once the filling ratio reaches high level. This may be attributed to the increased curvature and the decreased approachability with increasing layer thickness in the nanoporous channels. Consequently, adjusting the thickness of the ZnO layer resulting the control of void channels size in the periodically ordered multifunctional core-shell nanohybrids, providing a new way to calculate the nanoscale tubular wall thickness.

Composition control through alternating ALD processes.

Novel core-shell nanostructures can provide new materials for appealing applications. Yet, it is difficult to be fabricated from templated syntheses such as sol-gel reaction, electroplating and electroless plating by using BCPs as templates. For this purpose, ALD process was developed to fabricate nanomaterials with adjustable thickness for composite materials using alternating reaction, giving templated ALD with at least two gas precursors in a sequence. In this study, we demonstrate the fabrication of nanoporous core-shell metal oxide alloys through the templated ALD using the deposition of ZnO shell layer and Al₂O₃ core layer in the PS template as a model system. Fig. 6(a) displays [110] projected TEM micrograph of the PS/Al₂O₃@ZnO gyroid

nanohybrids deposited with ZnO for the first 40 ALD cycles followed by Al₂O₃ for 70 ALD cycles. After removing of PS matrix by calcination, the Al₂O₃@ZnO core-shell metal oxide alloys can be fabricated (Fig. 6(b)). To truly identify the formation of Al₂O₃ on ZnO *via* templated ALD, energy-dispersive X-ray spectroscopy (EDX) was acquired. In contrast to the characteristic peaks of the ZnO at

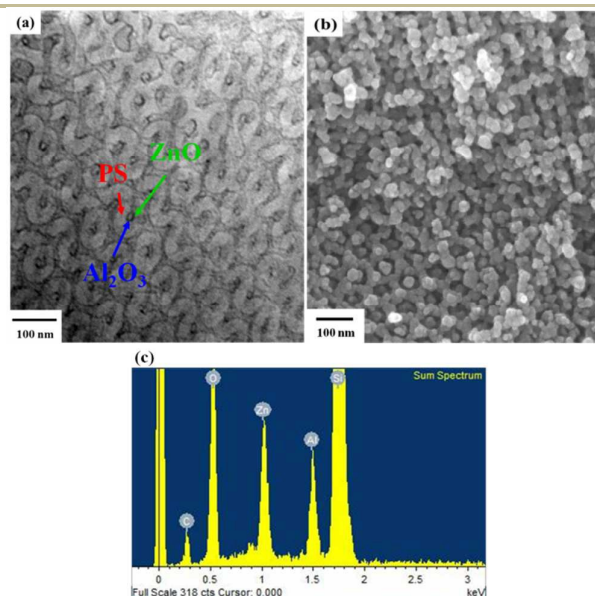


Fig. 6 Electron Microscopy images without staining: (a) TEM of PS/Al₂O₃@ZnO core-shell; (b) SEM of Al₂O₃@ZnO core-shell metal oxide alloy; (c) EDS of PS/Al₂O₃@ZnO gyroid nanohybrids.

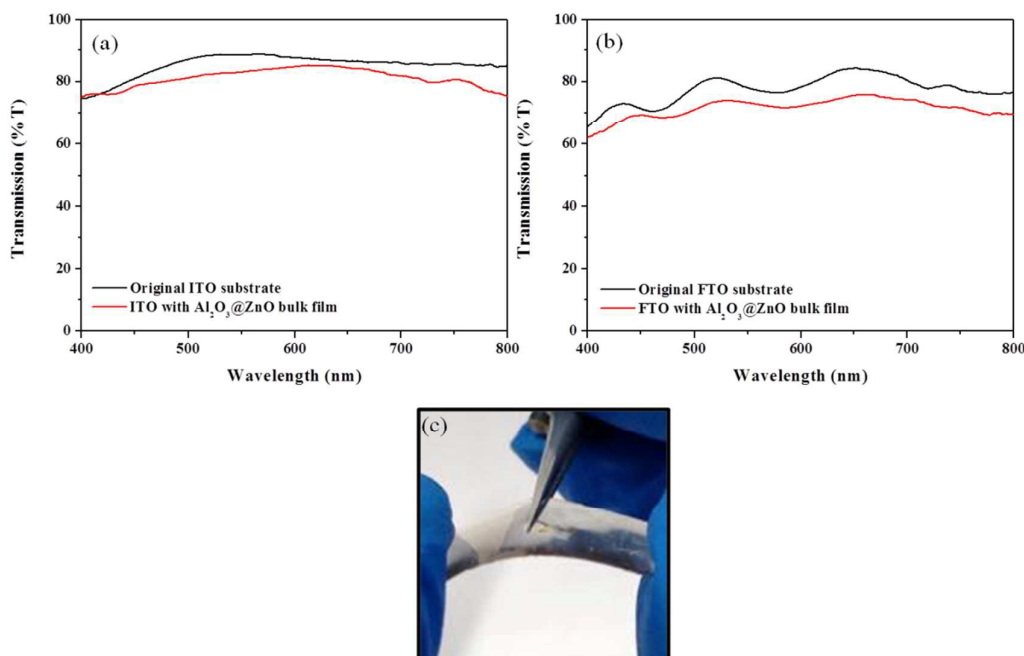


Fig. 7 UV-Vis transmission spectra of original substrates and Al₂O₃@ZnO thin film on (a) ITO and (b) FTO substrates. The photographs of (c) a 500 μm thickness thin film with gyroid networks held by a pair of tweezers and the film under bending, demonstrating its

mechanical robustness.

1.0 and 8.4 keV assigned to Zn° and the O° peaks at 0.6 keV, respectively, the characteristic peaks of the Al_2O_3 at 1.5 keV can be assigned to Al° and the O° peaks at 0.6 keV (Fig. 6(c)). Accordingly, the $\text{ZnO}/\text{Al}_2\text{O}_3$ core-shell nanostructure can be formed by this alternating reaction process for templated ALD. Note that the deposition rate of Al_2O_3 is approximately 1.3 Å per cycle which is different to the deposition rate of ZnO (approximately 2 Å per cycle).⁵¹ With the introduction of different gas precursors in sequence under controlled deposition rate, it is possible to fabricate the core-shell alloys with different combination of constituted metal oxides as demonstrated. Fig. S5 shows the large-field cross section view of a nanotube gyroid phase with entirely thickness of 5 µm by dip-coating method. The thick film was composed of ordered interconnected networks all over the total thickness of the film. Fig. S5 shows the zoom-in view of the nanoporous gyroid ZnO near the bottom side, in the middle, and near the surface, respectively. It cannot be observed apparent difference in the diameter and morphology for nanoporous gyroid structure located at different positions though these determined regions varied in the whole thin film. As a result, by taking advantage of ALD alternating reaction processes, novel core-shell nanostructures can be fabricated by using BCPs as templates, providing the new materials for potential applications in different research arenas.

Robust transparent films with network morphologies.

It is noted that the nanoporous ZnO with transparent character can be used for optical applications but its inferior mechanical properties are major drawbacks in practical uses. One of the efficient approaches to improve the required mechanical properties is to create core structure with tougher materials and then deposited with the shell ZnO for better optical performance.⁵² As demonstrated previously, it is possible to fabricate nanoporous alloys with core-shell texture (i.e., nanoporous gyroid $\text{Al}_2\text{O}_3@ZnO$). As shown in Fig. 7(a) and 7(b), the UV-Vis transmission spectra of the nanoporous gyroid $\text{Al}_2\text{O}_3@ZnO$ are basically equivalent to that of the neat ITO and FTO substrates with only less than 5% reduction in transmittance, indicating that the nanoporous gyroid $\text{Al}_2\text{O}_3@ZnO$ fabricated is nearly transparent as expected. We speculate that, in addition to the low absorption of the Al_2O_3 and ZnO over the whole spectral range of visible light, the high transparency might be attributed to the well-ordered gyroid texture in nanoscale that gives the low degree of scattering. For the demonstration of superior mechanical properties, a pair of tweezers was used to hold the nanoporous gyroid $\text{Al}_2\text{O}_3@ZnO$, and then the film was bended by hands as shown in Figures 7(c). As found, the nanoporous film is able to resist the bending and even twisting and no breaking and deformation can be observed after repeating mechanical stressing; namely, the nanoporous gyroid $\text{Al}_2\text{O}_3@ZnO$ is mechanically robust. As a result, free-standing network materials with high transmittance and robust mechanical properties can be fabricated due to its ordered isotropic nanostructure with tough Al_2O_3 core while the shell ZnO texture provides significant interactive surface

in the opto-electronics application due to the high specific surface area.

Conclusions

A novel platform technology using hydrolyzed BCP as a template for ALD to fabricate nanohybrids and nanoporous materials was developed in this study. By taking advantage of dip-coating approach for film formation, thin-film templates with micrometer thickness and open-cell character can be successfully fabricated, giving thin films with well-ordered co-continuous nanochannels after hydrolytic treatment. Consequently, nanohybrids with inorganic nanonetworks and nanoporous inorganics with free-standing character can be created through templated ALD. As demonstrated, PS/metal oxide gyroid nanohybrids (i.e., PS/ZnO gyroid nanohybrids) were fabricated. After removal of the PS matrix, micrometer-thick nanoporous gyroid ZnO can be obtained. Through the execution of controlled ALD cycles, it is feasible to provide nanoporous gyroid ZnO tube with tunable tube thickness as calculated by XRR measurements. Moreover, the formation of nanoporous metal oxide alloys with core-shell texture (e.g. $\text{Al}_2\text{O}_3@ZnO$) can be achieved by introducing the precursors for templated synthesis in sequence. Because of the high porosity and high specific surface area of the nanoporous gyroid metal oxides fabricated, it is highly promising to exploit the nanoporous materials interactive surface in the opto-electronics application.

Acknowledgements

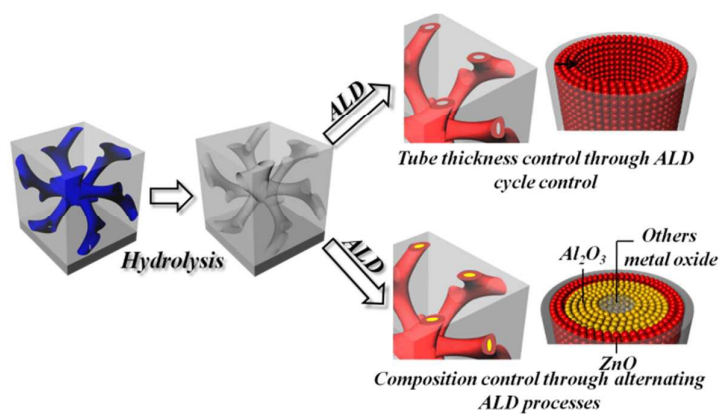
The authors would like to thank the National Science Council of the Republic of China, Taiwan, for financially supporting this research under Grant no. NSC 101-2221-E-007-038-MY3. The National Synchrotron Radiation Research Center (NSRRC) for its assistance in the Synchrotron SAXS experiments. We thank Mohan Raj Krishnan of the Department of Chemical Engineering at National Tsing Hua University for their help in editing the English writing.

References

- 1 Y. Deng, J. Wei, Z. Sun and D. Zhao, *Chem. Soc. Rev.*, 2013, **42**, 4054-4070.
- 2 R. C. Furneaux, W. R. Rigby and A. P. Davidson, *Nature*, 1989, **337**, 147-149.
- 3 P. Jiang, J. Cizeron, J. F. Bertone and V. L. Colvin, *J. Am. Chem. Soc.*, 1999, **121**, 7957-7958.
- 4 C. T. Kresge, M. E. Leonowicz, W. J. Roth, J. C. Vartuli and S. Beck, *Nature*, 1992, **359**, 710-712.
- 5 M. S. She, T. Y. Lo, H. Y. Hsueh and R. M. Ho, *NPG Asia Mater.*, 2013, **5**, e42.
- 6 H. Y. Hsueh, C. T. Yao and R. M. Ho, *Chem. Soc. Rev.*, 2015, **44**, 1974-2018.
- 7 G. M. Whitesides and B. Grzybowski, *Science*, 2002, **295**, 2418-2421.

- 8 E. L. Thomas, D. M. Anderson, C. S. Henkee and D. Hoffman, *Nature*, 1988, **334**, 598-601.
- 9 F. S. Bates and G. H. Fredrickson, *Phys. Today*, 1999, **52**, 32-38.
- 10 F. S. Bates, *MRS Bull.*, 2005, **30**, 525-532.
- 11 M. Park, C. Harrison, P. M. Chaikin, R. A. Register and D. H. Adamson, *Science*, 1997, **276**, 1401-1404.
- 12 V. Z. H. Chan, J. Hoffman, V. L. Lee, H. Iatrou, A. Avgeropoulos, N. Hadjichristidis, R. D. Miller and E. L. Thomas, *Science*, 1999, **286**, 1716-1719.
- 13 T. Thurn-Albrecht, R. Steiner, J. DeRouchey, C. M. Stafford, E. Huang, M. Bal, M. Tuominen, C. J. Hawker and T. P. Russell, *Adv. Mater.*, 2000, **12**, 1138-1138.
- 14 J. Y. Cheng, C. A. Ross, V. Z. H. Chan, E. L. Thomas, R. G. H. Lammertink and G. J. Vancso, *Adv. Mater.*, 2001, **13**, 1174-1178.
- 15 A. S. Zalusky, R. Olayo-Valles, C. J. Taylor and M. A. Hillmyer, *J. Am. Chem. Soc.*, 2001, **123**, 1519-1520.
- 16 R. M. Ho, W. H. Tseng, H. W. Fan, Y. W. Chiang, C. C. Lin, B. T. Ko and B. H. Huang, *Polymer*, 2005, **46**, 9362-9377.
- 17 V. Luzzati and P. A. Speg, *Nature*, 1967, **215**, 701-704.
- 18 A. H. Schoen, *NASA Technical Note*, TN D-5541, 1970.
- 19 D. A. Hajduk, P. E. Harper, S. M. Gruner, C. C. Honeker, G. Kim, E. L. Thomas and L. J. Fetters, *Macromolecules*, 1994, **27**, 4063-4075.
- 20 M. F. Schulz, F. S. Bates, K. Almdal and K. Mortensen, *Phys. Rev. Lett.*, 1994, **73**, 86-89.
- 21 M. W. Matsen and M. Schick, *Phys. Rev. Lett.*, 1994, **72**, 2660-2663.
- 22 W. H. Tseng, C. K. Chen, Y. W. Chiang, R. M. Ho, S. Akasaka and H. Hasegawa, *J. Am. Chem. Soc.*, 2009, **131**, 1356-1357.
- 23 H. Y. Hsueh, H. Y. Chen, M. S. She, C. K. Chen, R. M. Ho, S. Gwo, H. Hasegawa and E. L. Thomas, *Nano Lett.*, 2010, **10**, 4994-5000.
- 24 H. Y. Hsueh and R. M. Ho, *Langmuir*, 2012, **28**, 8518-8529.
- 25 E. J. W. Crossland, M. Kamperman, M. Nedelcu, C. Ducati, U. Wiesner, D. M. Smligies, G. E. S. Toombes, M. A. Hillmyer, S. Ludwigs, U. Steiner and H. J. Snaith, *Nano Lett.*, 2009, **9**, 2807-2812.
- 26 E. J. W. Crossland, S. Ludwigs, M. A. Hillmyer and U. Steiner, *Soft Matter*, 2010, **6**, 670-676.
- 27 S. Vignolini; N. A. Yufa, P. S. Cunha, S. Guldin, I. Rushkin, M. Stefik, K. Hur, U. Wiesner, J. J. Baumberg and U. Steiner, *Adv. Mater.*, 2012, **24**, OP23-OP27.
- 28 M. R. J. Scherer, L. Li, P. M. S. Cunha, O. A. Scherman, U. Steiner, *Adv. Mater.*, 2012, **24**, 1217-1221.
- 29 D. Wei, M. R. J. Scherer, C. Bower, P. Andrew, T. Ryhanen and U. Steiner, *Nano Lett.*, 2012, **12**, 1857-1862.
- 30 M. R. J. Scherer and U. Steiner, *Nano Lett.*, 2013, **13**, 3005-3010.
- 31 T. Hashimoto, K. Tsutsumi and Y. Funaki, *Langmuir*, 1997, **13**, 6869-6872.
- 32 I. Vukovic, S. Punzhin, Z. Vukovic, P. Onck, J. T. M. De Hosson, G. ten Brinke and K. Loos, *ACS Nano*, 2011, **5**, 6339-6348.
- 33 C. F. Cheng, H. Y. Hsueh, C. H. Lai, C. J. Pan, B. J. Hwang, C. C. Hu and R. M. Ho, *NPG Asia. Mater.*, 2015, **7**, e170
- 34 H. Y. Hsueh, R. M. Ho, Y. C. Huang C. H., Lai, T. Makida and H. Hasegawa, *Adv. Mater.*, 2011, **23**, 3041-3046.
- 35 H. Y. Hsueh, H. Y. Chen, Y. C. Huang, Y. C. Ling, S. Gwo and R. M. Ho, *Adv. Mater.*, 2013, **25**, 1780-1786.
- 36 Y. Wang, Y. Qin, A. Berger, E. Yau, C. C. He, L. B. Zhang, U. Gosele, M. Knez and M. Steinhart, *Adv. Mater.*, 2009, **21**, 2763-2766.
- 37 E. Kim, Y. Vaynzof, A. Sepe, S. Guldin, M. Scherer, P. Cunha, S. V. Roth and U. Steiner, *Adv. Funct. Mater.*, 2014, **24**, 863-872.
- 38 M. Agrawal, S. Gupta, A. Pich, N. E. Zafeiropoulos and M. Stamm, *Chem. Mater.*, 2009, **21**, 5343-5348.
- 39 H. Y. Hsueh, Y. C. Ling, H. F. Wang, L. Y. Chang Chien, Y. C. Hung, E. L. Thomas and R. M. Ho, *Adv. Mater.*, 2014, **26**, 3225-3229.
- 40 S. Salvatore, S. Vignolini, J. Philpott, M. Stefik, U. Wiesner, J. J. Baumberg and U. Steiner, *Nanoscale*, 2015, **7**, 1032-1036.
- 41 J. A. Dolan, B. D. Wilts, S. Vignolini, J. J. Baumberg, U. Steiner and T. D. Wilkinson, *Adv. Opt. Mater.*, 2015, **3**, 12-32.
- 42 X. W. D. Lou, L. A. Archer and Z. Yang, *Adv. Mater.*, 2008, **20**, 3987-4019.
- 43 X. B. Wang, T. Y. Lo, H. Y. Hsueh and R. M. Ho, *Macromolecules*, 2013, **46**, 2997-3004.
- 44 C. S. Ku; H. Y. Lee, J. M. Huang and C. M. Lin, *Mater. Chem. Phys.*, 2010, **120**, 236-239.
- 45 M. Ali and M. Winterer, *Chem. Mater.*, 2010, **22**, 85-91.
- 46 M. Agrawal, A. Pich, N. E. Zafeiropoulos, S. Gupta, J. Pionteck, F. Simon and M. Stamm, *Chem. Mater.*, 2007, **19**, 1845-1852.
- 47 J. W. Elam and S. M. George, *Chem. Mater.*, 2003, **15**, 1020-1028.
- 48 J. W. Elam, Z. A. Sechrist and S. M. George, *Thin Solid Films*, 2002, **414**, 43-55.
- 49 L. G. Parratt, *Phys. Rev.*, 1954, **95**, 359-369.
- 50 D. K. Bowen and B. K. Tanner, *J. Cryst. Growth*, 1993, **126**, 1-18.
- 51 M. D. Groner, F. H. Fabreguette, J. W. Elam and S. M. George, *Chem. Mater.*, 2004, **16**, 639-645.
- 52 Y. L. Chueh; C. H. Hsieh, M. T. Chang, L. J. Chou, C. S. Lao, J. H. Song, J. Y. Gan and Z. L. Wang, *Adv. Mater.*, 2007, **19**, 143-149

TOC



Here, we suggest an approach for the fabrication of nanoporous gyroid metal oxides with controlled tube thickness and composition by templated atomic layer deposition (ALD) using hydrolyzed block copolymers as templates. Controlled tube thickness can be achieved through the control of ALD cycle while alternating reaction processes can be carried out to provide controlled composition, giving nanoporous gyroid alloys with high porosity and large specific surface area as well as superior mechanical properties.